ELSEVIER

Chemical Engineering Journal 82 (2001) 311–328

Chemical Engineering Journal

www.elsevier.com/locate/cej

The kinetics of methane steam reforming over a Ni/α-Al_2O catalyst

Kaihu Hou, Ronald Hughes*

Chemical Engineering Unit, University of Salford, Maxwell Building, The Crescent, Salford, Manchester M5 4WT, UK

Received 26 May 2000; accepted 11 October 2000

Abstract

Experiments have been carried out to study the kinetics of the methane steam reforming, accompanied by the reverse water gas shift reaction over a commercial Ni/α-Al_2O_3 catalyst in an integral reactor under conditions of no diffusion limitation. The experiments demonstrated that both CO and CO_2 are formed as primary products, and the rate of methane disappearance is proportional to the partial pressure of methane at low product concentrations. The effect of total pressure on initial reaction rates indicated that the rate controlling steps of steam reforming are surface reactions between adsorbed species. Six possible reaction mechanisms were considered in detail, and intrinsic rate equations were derived by using the Langmuir–Hinshelwood–Hougen–Watson (LH–HW) approach and Freundlich's adsorption concept. Applying the method of parameter estimation and model discrimination, a satisfactory model of intrinsic kinetics for methane steam reforming over the catalyst used was determined. Good agreement was obtained between the experimental data and results predicted from the kinetic model.

Keywords: Intrinsic kinetics; Methane steam reforming; Nickel catalyst

1. Introduction

Methane steam reforming on solid catalysts is the well-established commercial process for the production of hydrogen and synthesis gas. The simulation and optimal design of the commercial process requires information on the intrinsic kinetics. A considerable effort has been put into investigations of the kinetics of methane steam reforming since the early 1950s [2,4–6,8–10,12,19,25,27]. Methane steam reforming is a quite complex process. It not only involves the transfer and diffusion of reactants and products between the bulk phase and catalyst surface as well as within the catalyst, but also involves several reactions simultaneously in parallel or in series. Since reported studies of the kinetics of the methane–steam reaction were carried out with catalysts of different compositions prepared by various methods and of different particle size, and over wide ranges of temperature and pressure, it is not surprising that different mechanisms and kinetics have been suggested. The reasons for this are two-fold (1) the change of catalyst composition changes not only the values of the parameters of the kinetic model, but it also changes the structure of the kinetic model via changes in the mechanism [25]; (2) the effects of the diffusion limitation in some experiments often results in misunderstanding of the kinetic mechanism [26]. This makes it impossible to develop generalised kinetics, which can be applied to different catalysts with only a change in parameters to suit each catalyst. Hence, it is necessary to study experimentally the mechanism and the kinetics for each type of steam reforming catalyst under conditions of no mass/heat transfer and diffusion limitations.

Reported kinetic rate equations can be roughly classified in two groups. The first group was concerned only with the kinetics of methane disappearance into carbon monoxide or carbon dioxide [1–3,8,9,21,17]. The second group accounted for the rates of carbon monoxide and carbon dioxide formation separately; from these predictions of product distribution may be made [5,12,20,25,27]. From the point of view of design, simulation and optimisation of an industrial reformer, detailed product compositions and effects of operational conditions on desired product yield should be determined. Hence, the second group of kinetic rate equations is more useful for this purpose.

The objective of this work is to study the intrinsic kinetics of the steam reforming of methane, accompanied by the reverse water gas shift reaction over a commercial Ni/α-Al_2O_3 catalyst in an integral reactor. Within wide ranges of temperature, pressure and steam:methane ratio, the effects of these parameters on reaction have been investigated experimentally in the absence of concentration and temperature differences between the fluid and solid phase.

In addition, the main reactions involved in methane steam reforming have been analysed thermodynamically and the

* Corresponding author. Tel.: +44-161-2955081; fax: +44-161-2955380.
E-mail address: r.hughes@salford.ac.uk (R. Hughes).

1385-8947/01/$ – see front matter
PII: S1385-8947(00)00367-3

Nomenclature

a_i, $a^{\bullet}_i$	correlation coefficients in Eqs. (3) and (7), respectively (kg cat s/kmol)$^{-1}$
A_i	pre-exponential factor of rate constant, k_i
$A(K_i)$	pre-exponential factor of adsorption constant, K_i
b_i, $b^{\bullet}_i$	correlation coefficients in Eqs. (4) and (8), respectively (kg cat s/kmol)$^{-1}$
E_i	activation energy of reaction i (kJ/mol)
F_i	molar flow rate of component i (kmol/s)
$\Delta H_{j,a}$	enthalpy change of adsorption (kJ/mol)
k_1, k_3	reaction rate constants of reactions (1) and (3), respectively (kmol/kg cat s) (kPa)$^{0.25}$
k_2	reaction rate constant of reaction (2) (kmol/kg cat s) (kPa)
K_{CH_4}	adsorption coefficient of CH_4 (kPa)$^{-1}$
K_{CO}	adsorption coefficient of CO (kPa)$^{-1}$
K_{H_2O}	adsorption coefficient of H_2O
K_{p_1}, K_{p_3}	equilibrium constant of reactions (1) and (3) (kPa)^2
K_{p_2}	equilibrium constant of reaction (2)
L	effective length of reactor (m)
P_i	partial pressure of component i (kPa)
P_t	total pressure (kPa)
r	reaction rate (kmol/kg cat s)
$r^{o}_{CH_4}$	rate of methane disappearance in steam reforming (kmol/kg cat s)
$r^{\bullet o}_{CH_4}$	rate of methane formation in reverse water gas shift reaction (kmol/kg cat s)
r^{o}_{CO}	rate of CO formation in steam reforming (kmol/kg cat s)
$r^{\bullet o}_{CO}$	rate of CO formation in reverse water gas shift reaction (kmol/kg cat s)
$r^{o}_{CO_2}$	rate of CO_2 formation in steam reforming (kmol/kg cat s)
$r^{\bullet o}_{CO_2}$	rate of CO_2 disappearance in reverse water gas shift reaction (kmol/kg cat s)
R	universal gas constant
s	active site of catalyst
T	temperature (K)
W	weight of catalyst (kg)
X_{CH_4}	methane conversion in steam reforming, and conversion of CO_2 into methane in reverse water gas shift reaction, respectively
X_{CO_2}	CO_2 conversion in reverse water gas shift reaction, and conversion of methane into CO_2 in steam reforming, respectively

Greek letters

α_{ij}	parameter in Eqs. (7)–(9)
ν_{ij}	stochiometric coefficient of component i in reaction j
ρ_B	density of catalyst bed (kg/m^3)
Ω	cross-sectional area of the catalyst bed (m^2)

Subscripts

i	component i, reaction i, or micropore
j	component j, or reaction j

Superscripts

i	inlet of reactor
o	outlet of reactor

effects of pressure and steam:methane ratio examined. A reaction mechanism for methane steam reforming is proposed, and kinetic rate equations have been developed by using the Langmuir–Hinshelwood–Hougen–Watson (LH–HW) approach and Freundlich's adsorption concept.

2. Equipment and materials

A schematic diagram of the experimental equipment used is given in Fig. 1. It consists of three sections: feed section, reaction section and analysis section. The feed section contains gas supplies for CH_4, CO_2, and H_2. After pressure reduction from the gas cylinder by means of a regulator, the flow rate of each gas was controlled by a mass flow controller at a desired value. After mixing the gases flowed into the preheater–evaporator in which the gas mixture was heated. Deionised water was delivered by a piston pump to the evaporator where it vaporised into steam and was mixed with the other gases in a predetermined ratio. The integral reactor and evaporator used in the present experiments were made from stainless steel tubes 1 cm i.d. enclosed by an electric resistance heater. A straight section, 338 mm long, served as the reactor, while the side arm section, 215 mm long, was used as the combined evaporator–preheater. A thermocouple was placed in a thermocouple well of 2 mm o.d. which was located along the axis of the reactor. The thermocouple was connected to a temperature indicator and a temperature controller to monitor and control the reaction temperature. Another thermocouple was located adjacent to the heating wire surrounding the evaporator to measure and control its temperature. After condensation of the steam and drying of the gas mixture, the effluent was sent to the analysis section. The analysis section contained the gas chromatograph (GC, Varian 3400) and the infra red gas analyser (Analytical Development Co., Ltd.). The GC with a thermal conductivity detector (TCD) and a column of 5 Å molecular sieve 2 m long was used to analyse the methane and carbon monoxide, and the infra red gas analyser was used to detect the carbon dioxide. The concentration of hydrogen in the effluent and the amount of steam consumed were determined by a hydrogen balance and an oxygen balance, respectively. Overall carbon balances were better than 95%.

The feed gases used were methane, carbon dioxide and hydrogen; the carrier gas for the GC used was helium. All

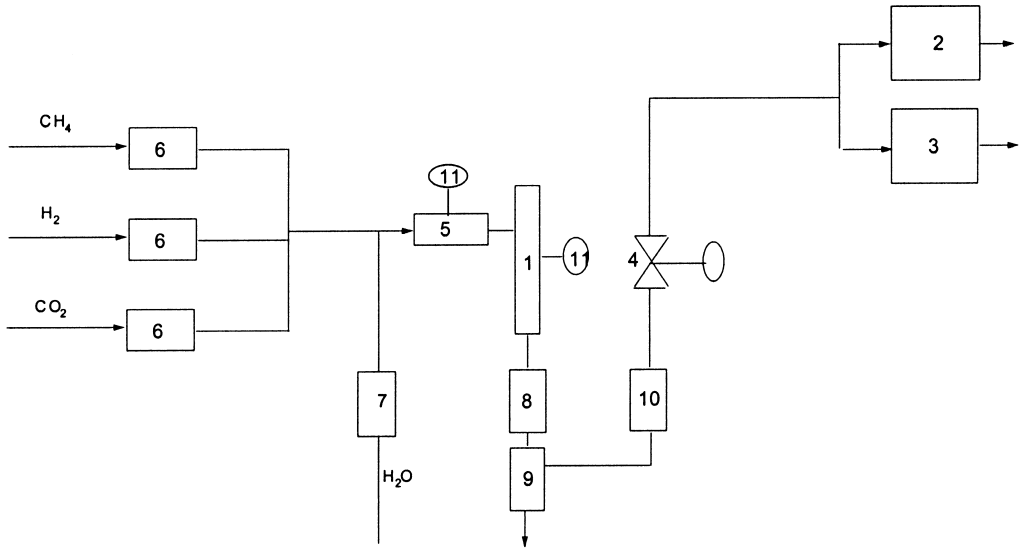

Fig. 1. Schematic of flow system methane steam reforming (integral reactor). 1: reactor; 2: gas chromatograph; 3: CO_2 analyser; 4: back pressure valve; 5: evaporator; 6: mass flow controller; 7: piston; 8: condenser; 9: gas–liquid separator; 10: dryer; 11: temperature controllers.

gases were purchased from BOC Ltd. and were of chemically pure grade (>99%).

3. Catalyst and its pre-treatment

A nickel/alumina catalyst (ICI steam reforming catalyst 57-4) of cylindrical type with four axial holes was provided by ICI Katalco. The physical properties of the catalyst are listed in Table 1 and the pore size profile is shown in Fig. 2. The original catalyst was crushed into particles of average diameter 0.15 mm to avoid intraparticle diffusion effects within present experimental condition, which was confirmed by the preliminary experiments mentioned later. The amounts of catalyst loaded were 0.3 and 0.1 g for the formal methane steam reforming reaction and the reverse water

Table 1
Catalyst properties

NiO content (%)	15–17
Surface area (BET, m^2/g)	14.30
Skeletal density (g/cm^2)	3.20
Geometric density (g/cm^2)	1.79
Pore volume (cm^3/g)	0.246
Porosity (cm^3/cm^3)	0.44

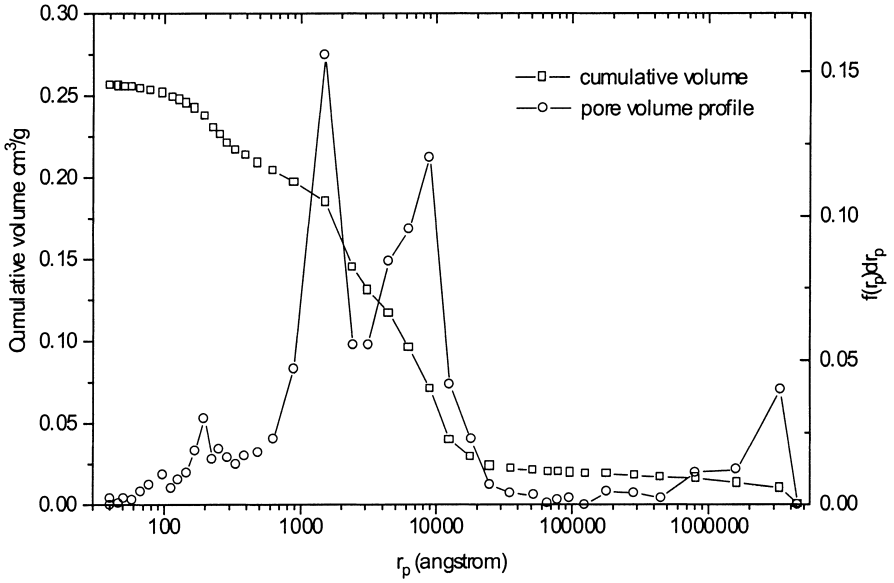

Fig. 2. Pore cumulative volume and pore volume profile of the catalyst.

gas shift reaction experiments, respectively. Once loaded, the catalyst was reduced by the following procedures (1) the catalyst was heated to 673 K at 3 K/min in nitrogen and maintained at this temperature for 1 h; (2) the catalyst was sustained at the same temperature for 2 h in hydrogen, and then it was heated to 873 K at 2.5 K/min and kept at this temperature for a further hour in hydrogen; (3) the temperature was decreased to the required operating temperature in a stream of hydrogen. The catalyst was then ready for the reaction experiments.

4. Preliminary experiments

Prior to the formal experiments, preliminary experiments were carried out to examine any catalyst deactivation and to find ways of maintaining the catalyst stability as long as possible, and to avoid any limitations of intraparticle diffusion.

Fig. 3 shows the variation of catalyst activity at different conditions with time. At reaction temperature of 823 K and reaction pressure of 120 kPa, with W/F_{CH_4} = 13356 kg cat s/kmol and molar ratio H_2O:CH_4 = 3:1 (run s1), it is clear that the catalyst activity decreases rapidly. Under such condition, the quality of the experimental data is unacceptable. At these experimental conditions, the rate of carbon formation on the catalyst should be quite slow. However, it was confirmed experimentally that small sized catalyst particles are quickly deactivated because reactions leading to carbon formation can easily occur in the interior of the catalyst particles [7]. Hence, the fast deactivation might be due to the use of a small size catalyst that had been chosen to minimise the effect of intraparticle diffusion. Based on a thermodynamic analysis of possible carbon formation reactions, it was found that the catalyst deactivation resulted mainly from methane decomposition. To inhibit this reaction, hydrogen, one of products of this reaction, may be added to the feed. By increasing the hydrogen:methane molar ratio in the feed by small steps, an acceptable equimolar ratio of hydrogen to methane was determined. At this ratio, other reaction conditions, such as temperature, pressure and the molar ratio of steam:methane could be varied over wider ranges. Fig. 3 also shows the improvement of catalyst deactivation with time at P_t = 120 kPa, W/F_{CH_4} = 13356 kg cat s/kmol, at a molar ratio of H_2O:CH_4:H_2 = 5.5:1:1, and T = 798 K (experimental runs s3, and s5) and 823 K (experimental run s4 and s7), respectively. The activity of the catalyst still drops noticeably during the first 200 min, but then more slowly. After 250 min, the deactivation has become so slow that only minor corrections, as explained later, were necessary to apply to the experimental data to account for it. The experimental data, for the kinetic study under specific conditions, were collected during times from 270 to 450 min on stream. For the reverse water gas shift reaction, stabilised activities of fresh and used catalysts were obtained due to a low temperature used with less risk of carbon formation from this reaction. The data for the reverse water gas shift experiments were collected at 200–400 min on stream.

To guarantee that the experiments were carried out within a region of intrinsic kinetics, the effect of intraparticle and external film diffusion on methane steam reforming was examined by using five different average sizes of catalyst particles (0.608, 0.440, 0.253, 0.150, 0.105 mm) at conditions of P_t = 120 kPa, W/F_{CH_4} = 22250 kg cat s/kmol, a molar ratio of H_2O:CH_4:H_2 = 4:1:1 and temperatures ranging from 748 to 823 K. It was found that there are no significant changes in values of the methane conversion for the last two particle sizes. This result indicates that both the intraparticle diffusion limitation and that of film resistance is negligible for particles of 0.15 mm or less within

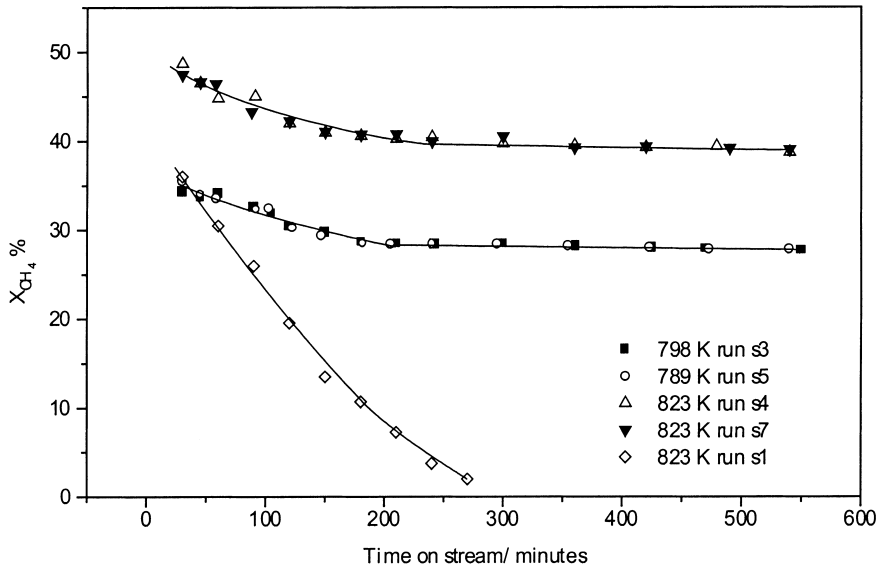

Fig. 3. Variation of catalyst activity with time.

Table 2
Experimental conditions

Pressure (kPa)	Temperature (K)	H_2O:CH_4:H_2 molar ratio
Methane steam reforming experiments		
120	748, 773, 798, 823	4:1:1
120	748, 773, 798, 823	5.5:1:1
300	748, 773, 798, 823	5.5:1:1
450	798, 823	5.5:1:1
600	748, 773, 798, 823	5.5:1:1
120	748, 773, 798, 823	7:1:1
Reverse water gas shift experiments		H_2/CO_2 (molar ratio)
120	598, 623, 648, 673	0.75
120	598, 623, 648, 673	0.5

the present temperature range. Consequently, for the main experiments, catalyst particles of 0.12–0.18 mm (average diameter 0.15 mm) were used.

Also applying methods suggested by Satterfield [24], the temperature difference and relative concentration difference between fluid phase and solid phase were confirmed as ca. 1 K and 0.2%, respectively. Hence, effects of the heat and mass transfer on reactions can be neglected in the present experiments.

5. Experimental results and discussion

The thermodynamic relationships for methane steam reforming limit any kinetic study to a rather narrow temperature range [2]. Also reaction pressure and total flow rate are limited by the equipment. The conditions chosen for the experiments are listed in Table 2. Based on the catalyst stability experiments, a mode of operation which enabled runs to be completed within 1 day was chosen, but using fresh catalyst due to its slow deactivation. To account for effects of the slow deactivation on the experiments, the reference conditions chosen for methane steam reforming were $P_t = 120\,\text{kPa}$, $W/F_{CH_4} = 13356\,\text{kg cat s/kmol}$, a molar ratio of H_2O:CH_4:H_2 = 5.5:1:1 and $T = 798\,\text{K}$. For the reverse water gas shift reaction, the conditions were $P_t = 120\,\text{kPa}$, $W/F_{CO_2} = 1800\,\text{kg cat s/kmol}$, a molar ratio of H_2:CO_2 = 0.75:1, and $T = 673\,\text{K}$.

Test under reference conditions was carried out for each experiment, prior to runs at other conditions. A minor correction on slow catalyst deactivation was done by correcting the contact time. The contact time of the test was assigned a $(W_{cat}/F_{CH_4})_1$ value at the beginning of each set of experiments. When the data collection was finished, the contact time $(W_{cat}/F_{CH_4})_2$ for obtaining the same conversion as at the beginning was determined. The correction factor for contact time due to the catalyst deactivation is given by

$$f_c = 1 - \frac{t}{t_{1-2}}\left[1 - \frac{(W_{cat}/F_{CH_4})_1}{(W_{cat}/F_{CH_4})_2}\right] \quad (1)$$

where t is time for collecting data from the beginning of the test, series up to the time of a particular sample analysis, and t_{1-2} is total time duration for the overall number of samplings. The corrected contact time is then

$$\left(\frac{W_{cat}}{F_{CH_4}}\right)_c = f_c \frac{W_{cat}}{F_{CH_4}} \quad (2)$$

Values for f_c were between 0.97 and 1.0.

For convenience, the corrected contact time is still termed the contact time, and is expressed as W_{cat}/F_{CH_4} hereafter.

5.1. The effects of temperature, pressure and ratio of steam:methane on methane conversion

Typical methane conversions versus contact time for different steam:methane ratio are shown in Figs. 4 and 5. Except for the positive effect of temperature on methane conversion found, two other main observations may be noted from the figures. First, the temperature effect is augmented as temperature increases. In other words, the effect of temperature on methane conversion is non-linear relationship between reaction rate constants and temperature. Secondly, when methane conversion is low, methane conversion is almost proportional to contact time at a constant ratio of steam:methane. Comparing the figures, it is also found that this proportional trend is enhanced by an increase in the steam:methane ratios. This indicates that the rate of methane disappearance is proportional to the partial pressure of methane at low product concentrations, due to insignificant back reaction.

Methane steam reforming is sensitive to pressure. High pressure not only enhances the forward reaction rates but also greatly enhances the backward reaction rates. Thus, a high applied pressure will not benefit methane steam reforming with regard to methane conversion. Under the present conditions, Fig. 4 shows a positive effect of pressure on methane conversion. This is due to the low temperatures used and the low product concentrations obtained in the experiments, and also because the enhancement of the forward reaction rates with pressure increase is larger than that of the backward reaction rates at these temperatures. A comparison of these effects between two different temperatures is presented in Fig. 5, indicating the decreased significance of these effects with temperature and contact time due to a larger enhancement of the backward reaction rates at the high product concentrations. This is consistent with the thermodynamics and kinetics of methane steam reforming.

5.2. The effects of temperature, pressure and the ratio of steam:methane on product distribution

Many reactions are involved in methane steam reforming. The operating conditions, such as temperature, pressure and the steam:methane ratio greatly affect the product composition. In most industrial cases, the product composition approaches the equilibrium composition which depends on

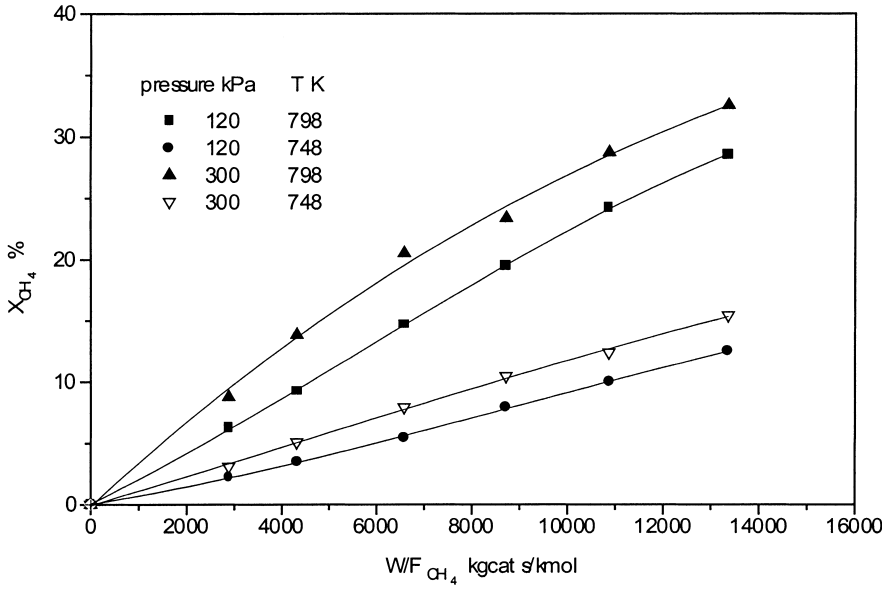

Fig. 4. The effects of reaction pressure on methane conversion, H_2O:CH_4:H_2 = 5:1:1.

the operating conditions at the exit of reformer as well as on the feed composition. For such cases, the influence of these operational parameters on the product composition, i.e. product distribution, depends on the thermodynamics of the reactions. It is of benefit in a study of the reaction kinetics to examine the effects of operational parameters on the product distribution far from the equilibrium conversion.

Fig. 6a shows the variation of carbon dioxide selectivity, defined as a molar number ratio of CO_2 produced to CH_4 converted from which the product distribution can be determined. An almost linear decrease of the selectivity with conversion increase was observed from the figure at constant temperature and constant steam:methane ratio. A possible reason for this decrease is that carbon dioxide is converted to carbon monoxide via the reverse water gas shift reaction. The high selectivity obtained at low methane conversions suggests that the main primary product is carbon dioxide. However, with the selectivities being less than one at low conversions, this also means that carbon monoxide is one primary product of the reactions. It is also found that the selectivity drops as temperatures increase. This may result from the different effect of temperature on those reactions which produce carbon dioxide, and those which produce carbon monoxide. Based on the decreased trend of selectivity

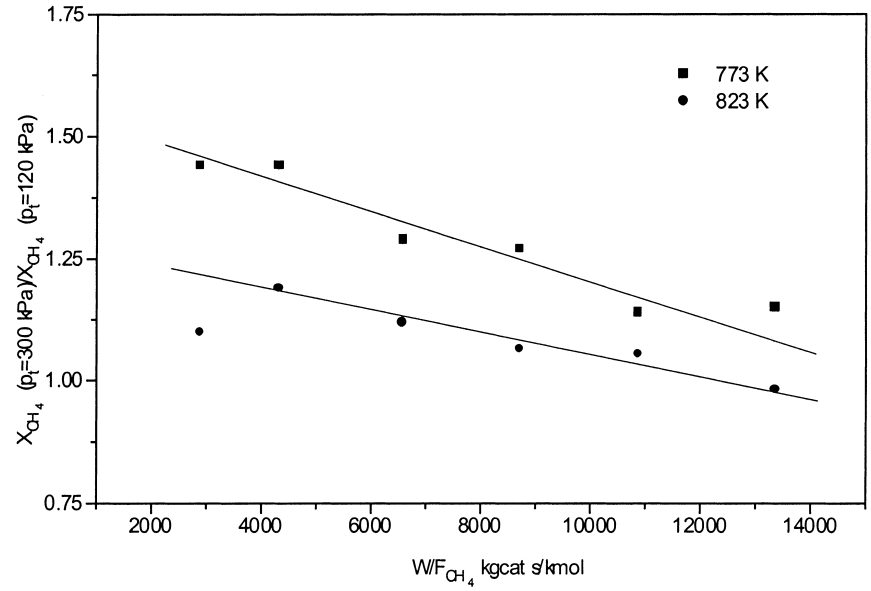

Fig. 5. The variation of the effect of pressure on methane conversion H_2O:CH_4:H_2 = 5:1:1.

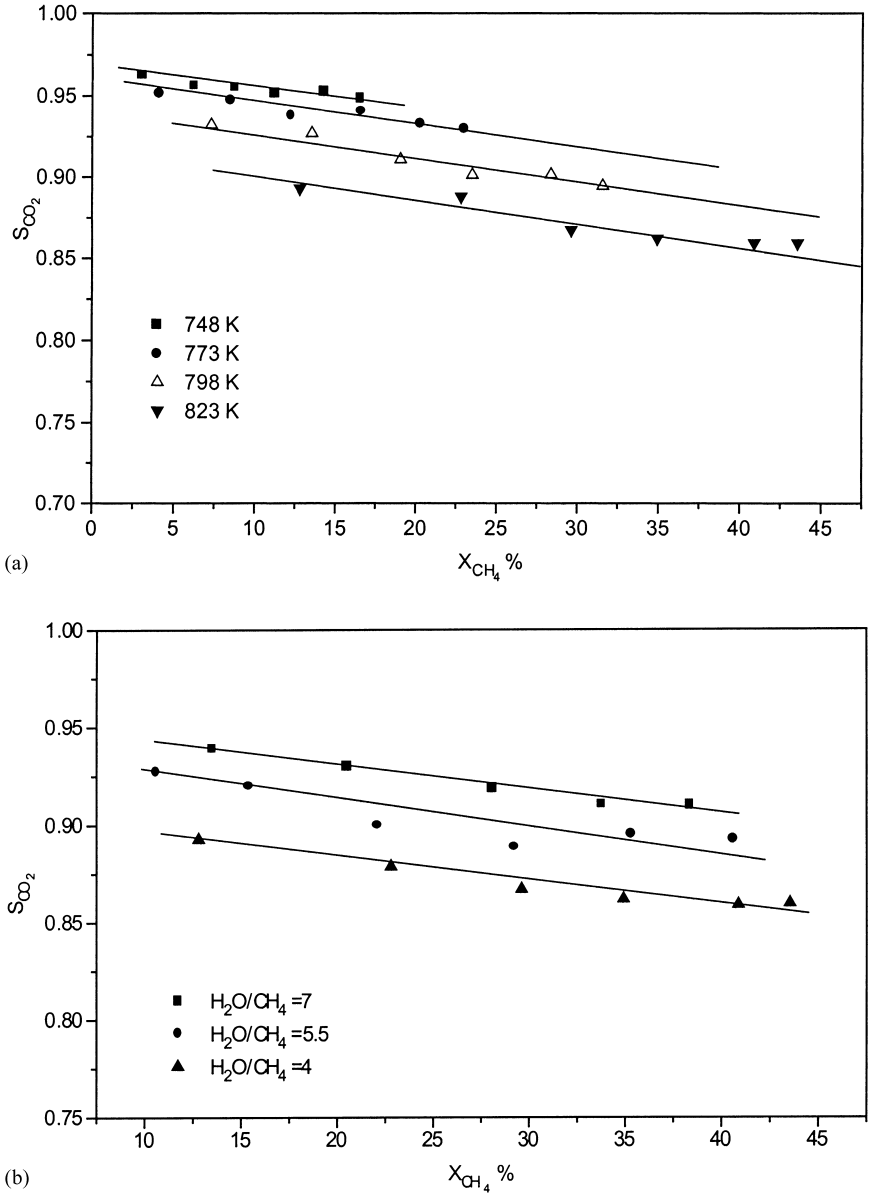

Fig. 6. (a) Selectivity of carbon dioxide vs. methane conversion, H_2O:CH_4:H_2 = 4:1:1, P_t = 120 kPa, T = 823 K. (b) The effect of the H_2O:CH_4 ratio on the selectivity of carbon dioxide, P_t = 120 kPa, T = 823 K.

with temperature increase, it can be expected that both carbon dioxide and carbon monoxide will be the main primary products at high temperature.

An increase of the steam:methane ratio causes a selectivity increase as shown in Fig. 6b. High concentrations of steam are favourable to reactions which produce carbon dioxide from methane directly, and inhibit the reverse water gas shift reaction that consumes carbon dioxide. This is one of the considerations that justify the use of surplus steam for manufacture of hydrogen and synthesis gas.

No noticeable effect of pressure on the selectivity was obtained. This may be because methane steam reforming is first-order with respect to the partial pressure of methane, and surplus steam is used, as well as the fact that experiments were carried out at low methane conversions in the present investigation.

5.3. Discussion on the reverse water gas shift experiments

As the water gas shift reaction is essentially at thermodynamic equilibrium during methane steam reforming at high temperature [25], it is helpful to carry out the reverse water gas shift reaction at low temperatures in order to obtain more accurate estimates for the kinetic parameters of the water gas shift reaction on the same catalyst.

Two different feed compositions were used to study this reaction and each was run at four different temperatures. The experimental data for each feed composition were

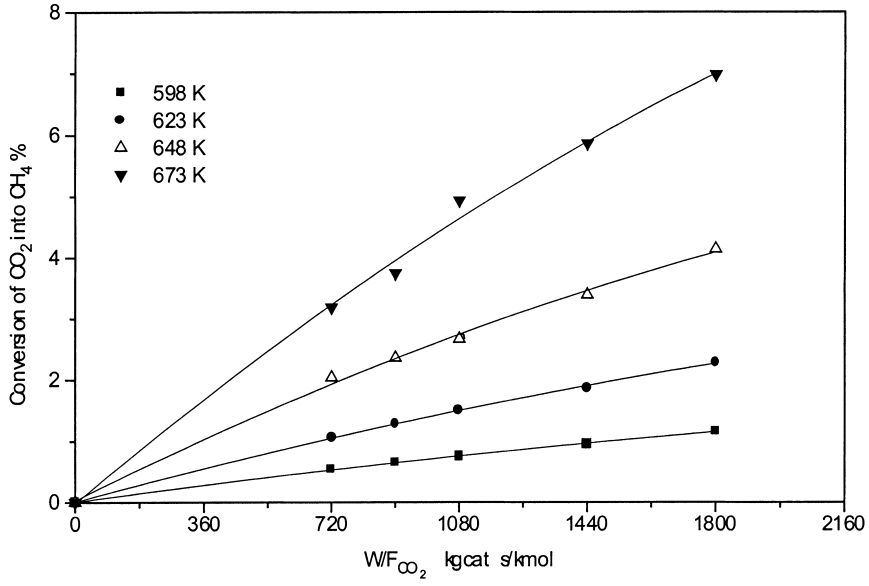

Fig. 7. Conversion of carbon dioxide into methane vs. contact time W/F_{CO_2} $P_t = 120\,kPa$, $H_2{:}CO_2 = 75$.

collected at one catalyst loading since the activity of the catalyst used was restored by hydrogen re-reduction. Minor corrections of experimental data due to slow catalyst deactivation were taken into account in the same way as for methane steam reforming described above. The monotonic increase of conversion of carbon dioxide into methane with contact time at $P_t = 120\,kPa$ and $H_2{:}CO_2 = 0.75$ for different temperatures is exhibited in Fig. 7. The methane could be produced either from reaction with carbon dioxide and hydrogen directly or from reaction with carbon monoxide and hydrogen indirectly, and the concentration of steam produced was so low that the methane steam reforming reaction is unimportant, compared with reactions which produced methane. As carbon monoxide is not only a product of reverse water gas shift reaction, but also is a reactant to produce methane, a non-monotonic change of the conversion of carbon dioxide into carbon monoxide is expected at high conversions of carbon dioxide and high reaction temperatures as shown in Fig. 8.

6. Thermodynamic analysis

The overall reaction of methane and steam to form carbon, carbon monoxide, carbon dioxide and hydrogen may be presented by the equations listed in Table 3 [2,13,27].

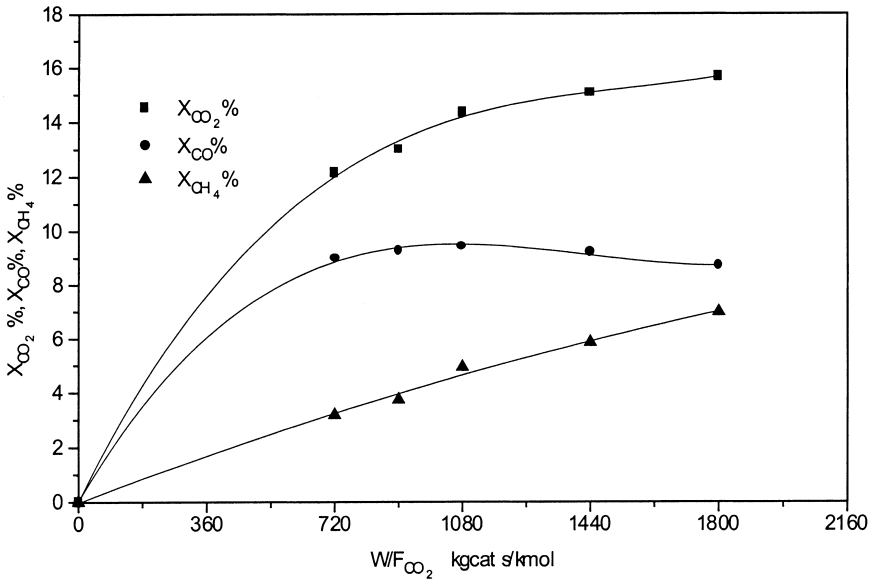

Fig. 8. Distribution of X_{CO_2}, X_{CO}, X_{CH_4}, $P_t = 120\,kPa$, $H_2{:}CO_2 = 0.75$, $T = 673\,K$.

Table 3
Reaction equations and equilibrium constants

I	Reaction	K_{p_i}	Dimensions
1	$CH_4 + H_2O = CO + 3H_2$	$1.198 \times 10^{17} \exp(-26830/T)$	$(kPa)^2$
2	$CO + H_2O = CO_2 + H_2$	$1.767 \times 10^{-2} \exp(4400/T)$	$(kPa)^0$
3	$CH_4 + 2H_2O = CO_2 + 4H_2$	$2.117 \times 10^{15} \exp(-22430/T)$	$(kPa)^2$
4	$CH_4 + CO_2 = 2CO + 2H_2$	$6.780 \times 10^{18} \exp(-31230/T)$	$(kPa)^2$
5	$CH_4 + 3CO_2 = 4CO + 2H_2O$	$2.170 \times 10^{22} \exp(-40030/T)$	$(kPa)^2$
6	$CH_4 = C + 2H_2$	$4.161 \times 10^{7} \exp(-10614/T)$	kPa
7	$2CO = C + CO_2$	$5.744 \times 10^{-12} \exp(20634/T)$	$(kPa)^{-1}$
8	$CO + H_2 = C + H_2O$	$3.173 \times 10^{-10} \exp(16318/T)$	$(kPa)^{-1}$
9	$CO_2 + 2H_2 = C + 2H_2O$	$1.753 \times 10^{-8} \exp(12002/T)$	$(kPa)^{-1}$
10	$CH_4 + 2CO = 3C + 2H_2O$	$4.190 \times 10^{-12} \exp(22022/T)$	$(kPa)^{-1}$
11	$CH_4 + CO_2 = 2C + 2H_2O$	$0.730 \exp(1388/T)$	$(kPa)^0$

From the standpoint of the thermodynamics of a reaction system, a ratio

$$V_i = \frac{\left(\prod_j p_j^{v_j}\right)_i}{K_{p_i}}$$

calculated from the experimental results, can determine the possible direction of a given reaction. If V_i is less than 1, reaction i is proceeding to the right, otherwise the reaction has a tendency to go to the left. Figs. 9 and 10 show the distributions of V_i with reaction extent at $P_t = 120$ kPa, $T = 823$ K, and a steam:methane:hydrogen ratio of 5.5:1:1. Similar results were obtained from experiments on methane steam reforming at other conditions. From Fig. 9, it can be seen that V_i for reactions (1), (3), (4) and (5) increase monotonically with reaction extent and are always smaller than one up to 40% of conversion of methane. This indicates that these reactions should proceed to the right in terms of thermodynamics. Since the observed methane disappearance rate decreased as methane conversion increased and, therefore, the carbon dioxide concentration increased, the rates of reactions (4) and (5) could be quite slow in contrast with the V_4 and V_5 values. Thus, reactions (4) and (5) were not considered to occur from the viewpoint of kinetic analysis. The V_2 and V_6 distributions with reaction extent are presented in Fig. 10. The V_2 distribution suggests that reaction (2) should proceed to the right initially at low extents of reaction, and then reverse to the left as the reaction extent increased. This means that part of the carbon monoxide was produced from reaction (2) at high reaction extents. Possible carbon formation caused by the methane decomposition reaction (6) is indicated when V_6 is less than 1 at low extents of reaction as shown in Fig. 10. Large positive values of V_i were obtained for reactions (7)–(11). This confirms that carbon formation is unlikely from these reactions. If these reactions were involved in methane steam reforming, they would progress to

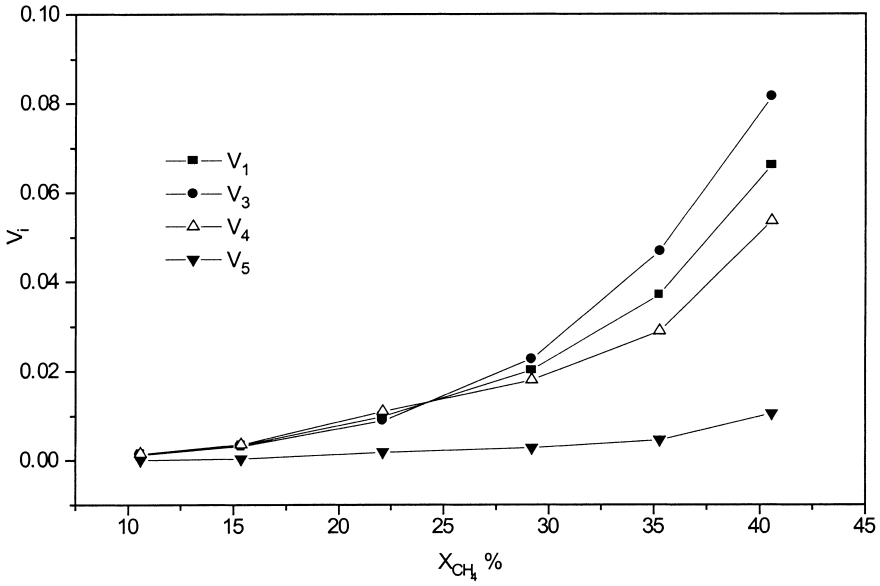

Fig. 9. V_i distribution with reaction extent, reactions (1), (3), (4) and (5).

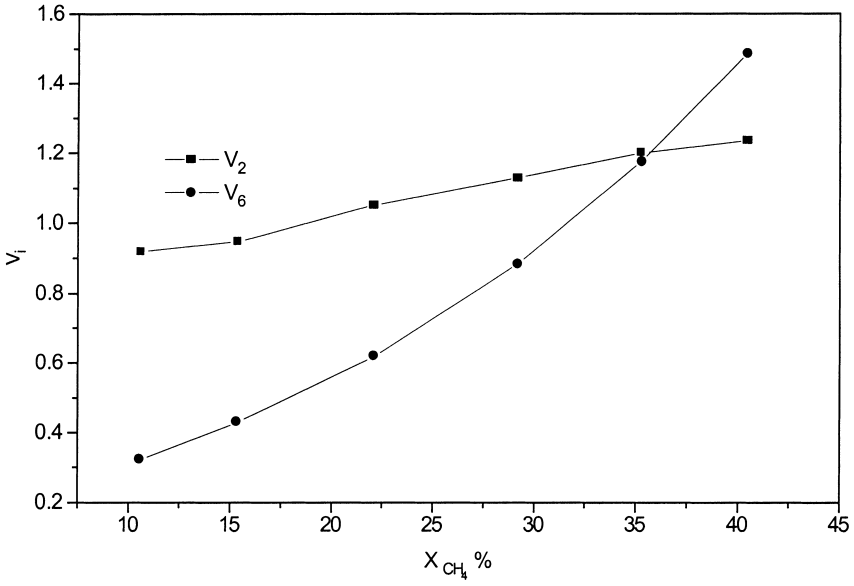

Fig. 10. V_i distribution with reaction extent, reactions (2) and (6).

the left according to thermodynamics under the present experimental conditions.

A similar analysis may be applied to the data on the reverse water gas shift experiments since the reactions listed in the Table 3 may be involved in these. The V_i values exceeded one for reactions (1)–(5) suggesting that these reactions tend to go to the left. Since the carbon dioxide concentration decreased monotonically as contact time increased, the effects of reactions (4)–(5) proceeding to the left on the process mass balance would not be meaningful. Among the six reactions involving carbon, five reactions (7)–(11) proceed to the right and could yield carbon, as their V_i values were much smaller than one, whereas reaction (6) displayed a tendency to proceed to the left, which might play a role in decoking to some extent. During the reverse water gas shift experiments, it was found that there was no noticeable carbon formation on the catalyst; hence this would not significantly affect the mass balance for the kinetics under consideration. Based on the thermodynamic analysis above, the process of methane steam reforming, and the reverse water gas shift can be described on the basis of reactions (1)–(3) for the study of the intrinsic kinetics.

7. Effects of pressure and steam:methane ratio on the rates of reactions

Methane steam reforming consists of a series of steps: reactants are adsorbed on the catalyst surface with or without dissociation, surface reactions occur between reactants adsorbed or between reactants adsorbed and reactants in the gas phase, and finally desorption of products occurs. In general, there are one or more slower steps, which control the total reaction in methane steam reforming. The determination of the rate controlling step is helpful in postulating a kinetic mechanism and in deriving the rate equations. An analysis of the effects of operating conditions on the initial reaction rate can provide some meaningful clues for guessing the rate controlling steps. For instance, the effect of total pressure or partial pressure (i.e. concentration), on initial reaction rate has been used for determining the rate controlling steps for several types of reaction [15].

8. Experimental reaction rate derivations

Second or third degree polynomial regressions were used for correlating relationships between methane conversion and contact time, and between conversion of methane into carbon dioxide and contact time, respectively. The relationships for the experiments of methane steam reforming at a fixed temperature, pressure and the ratio of steam:methane:hydrogen were obtained as follows:

$$X_{CH_4} = a_0 + a_1\left(\frac{W}{F_{CH_4}}\right) + a_2\left(\frac{W}{F_{CH_4}}\right)^2 + a_3\left(\frac{W}{F_{CH_4}}\right)^3 \quad (3)$$

$$X_{CO_2} = b_0 + b_1\left(\frac{W}{F_{CH_4}}\right) + b_2\left(\frac{W}{F_{CH_4}}\right)^2 + b_3\left(\frac{W}{F_{CH_4}}\right)^3 \quad (4)$$

Some of the a_i and b_i are listed in Table 4.

By differentiating Eqs. (3) and (4), the methane disappearance rate and carbon dioxide formation rate can be given,

Table 4
Correlation of conversion data

	Temperature (K)	$a_0(b_0) \times 10^2$	$a_1(b_1) \times 10^5$	$a_2(b_2) \times 10^9$	$a_3(b_3) \times 10^{13}$
$P_t = 120$ kPa, H_2O:CH_4:H_2 = 4:1:1					
X_{CH_4}	748	0.03690	1.2471	−0.1444	
	773	−0.02036	2.1734	−0.3102	
	798	0.1332	3.4292	−0.8011	
	823	0.6764	5.7203	−1.8931	
X_{CO_2}	748	0.01887	1.2009	−0.1499	
	773	−0.1745	2.0620	−0.3210	
	798	0.1886	3.1553	−0.7882	
	823	0.7589	4.9861	−1.6971	
$P_t = 120$ kPa, H_2O:CH_4:H_2 = 5.5:1:1					
X_{CH_4}	748	−0.05345	0.7894	−0.06790	
	773	−0.2194	1.5294	−0.01696	
	798	−0.2591	2.4181	−0.1373	
	823	0.8996	3.6050	−0.08804	−0.2510
X_{CO_2}	748	0.04759	0.7639	−0.06102	
	773	−0.1881	1.4465	−0.01090	
	798	−0.2170	2.2337	−0.1627	
	823	0.1230	3.3117	−0.1341	−0.2330
$P_t = 120$ kPa, H_2O:CH_4:H_2 = 7.0:1:1					
X_{CH_4}	748	−0.04810	0.7697	−0.04120	
	773	−0.1045	1.3687	−0.04445	
	798	−0.1006	2.0453	−0.1580	
	823	0.02009	2.5509	1.6934	−1.0892
X_{CO_2}	748	−0.04776	0.7618	−0.02877	
	773	−0.09124	1.3228	−0.04865	
	798	−0.08179	1.9766	−0.1863	
	823	0.1161	2.5386	1.2192	−0.8730

respectively, as

$$r_{CH_4} = \frac{dX_{CH_4}}{d(W/F_{CH_4})} = a_1 + 2a_2\left(\frac{W}{F_{CH_4}}\right) + 3a_3\left(\frac{W}{F_{CH_4}}\right)^2 \quad (5)$$

$$r_{CO_2} = \frac{dX_{CO_2}}{d(W/F_{CH_4})} = b_1 + 2b_2\left(\frac{W}{F_{CH_4}}\right) + 3b_3\left(\frac{W}{F_{CH_4}}\right)^2 \quad (6)$$

Similarly, applying the procedures above to the reverse water gas shift experiments, the carbon dioxide disappearance rate and methane formation rate can be obtained from

$$r^{\bullet}_{CO_2} = \frac{dX^{\bullet}_{CO_2}}{d(W/F_{CO_2})} = a^{\bullet}_1 + 2a^{\bullet}_2\left(\frac{W}{F_{CO_2}}\right) + 3a^{\bullet}_3\left(\frac{W}{F_{CO_2}}\right)^2 \quad (7)$$

$$r^{\bullet}_{CH_4} = \frac{dX^{\bullet}_{CH_4}}{d(W/F_{CO_2})} = b^{\bullet}_1 + 2b^{\bullet}_2\left(\frac{W}{F_{CO_2}}\right) + 3b^{\bullet}_3\left(\frac{W}{F_{CO_2}}\right)^2 \quad (8)$$

8.1. Effects of steam:methane ratio and pressure on initial reaction rates

Letting $W/F_{CH_4} = 0$, the initial methane disappearance rate can be derived from Eq. (5).

Fig. 11 shows the effect of steam:methane ratio on the initial methane disappearance rates at $P_t = 120$ kPa, and different temperatures. As seen in this figure, the initial methane disappearance rate decreased as the steam concentration increased, even though steam served as a reactant in methane steam reforming, and the effect of steam:methane ratio on the initial methane disappearance rate increased with temperature increase. The reasons for this are (1) the increase of steam concentration actually decreased the methane partial pressure for a given reaction pressure and the methane disappearance rate is first-order with respect to methane as confirmed by most investigators ([2,9,17,22,27] and for low conversions in the present work, Figs. 4 and 5); (2) the high steam concentration hinders methane from adsorbing on the catalyst surface, particularly at high temperatures as high temperature is favourable for water vapour adsorption with dissociation on the catalyst surface.

The effects of total pressure on initial methane disappearance rates are presented in Fig. 12 at ratios of steam:methane:hydrogen = 5.5:1:1 and for different temperatures. It is clear that the initial methane disappearance

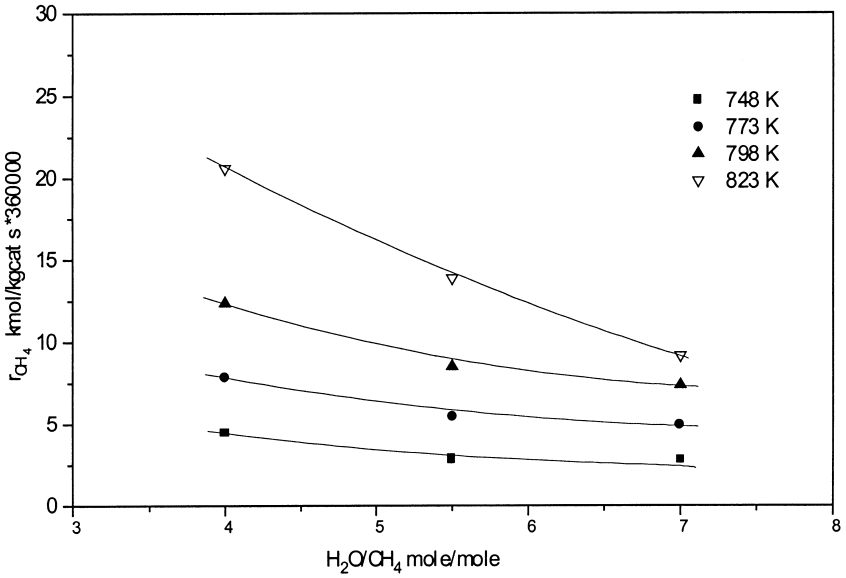

Fig. 11. Effect of ratio of steam:methane on initial methane disappearance rate.

rates increased slightly as pressure increased. Hence, it can be concluded that the desorption of products is not the rate controlling step of steam reforming. Comparing this figure with the figures presented by Froment and Bischoff [15], suggests that surface reactions are rate controlling during methane steam reforming.

9. Model development

9.1. Mechanisms and reaction rate equations of methane steam reforming

Because a mechanism of steam or methane in the gas phase reacting with adsorbed reactants is not generally accepted by most investigators, the following possibilities for the mechanism of methane steam reforming on different catalysts under different conditions can be considered [25].

Steam: (a_1) steam is adsorbed on the catalyst

$$H_2O + s = H_2O(s)$$

(a_2) steam is adsorbed on the catalyst with dissociation

$$H_2O + s = H_2 + O(s)$$

Methane: (b_1) methane is adsorbed on the catalyst

$$CH_4 + s = CH_4(s)$$

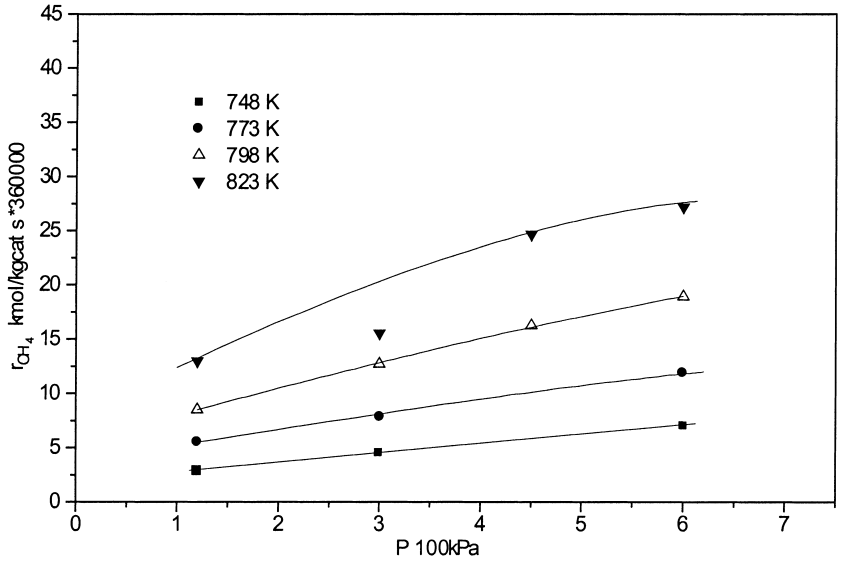

Fig. 12. Effect of pressure on initial methane disappearance, H_2O:CH_4:H_2 = 5.5:1:1.

Table 5
Descriptions of the kinetic mechanisms and combinations

Kinetic mechanism	Combination	Description
1	(a_1) and (b_1)	Steam and methane adsorbed on the catalyst, respectively
2	(a_1) and (b_2)	Steam adsorbed on the catalyst and methane absorbed on the catalyst with dissociation into CH_2 and H_2 or adsorbed H
3	(a_1) and (b_3)	Steam absorbed on the catalyst and methane absorbed on the catalyst with dissociation into C and H_2 or absorbed H
4	(a_2) and (b_1)	Methane absorbed on the catalyst and steam adsorbed on the catalyst with dissociation into H_2 and adsorbed O
5	(a_2) and (b_2)	Both methane and steam adsorbed on the catalyst with dissociation; methane dissociated into CH_2 and H_2 or adsorbed H
6	(a_2) and (b_3)	Both methane and steam adsorbed on the catalyst with dissociation, but methane dissociated into C and H_2 or adsorbed H

(b_2) methane is adsorbed on the catalyst with dissociation into H_2 and CH_2

$$CH_4 + s = CH_2(s) + H_2 \text{ or } CH_4 + 3s = CH_2(s) + 2H(s)$$

(b_3) methane is adsorbed on the catalyst with dissociation into H_2 and C

$$CH_4 + s = C(s) + 2H_2 \text{ or } CH_4 + 5s = C(s) + 4H(s)$$

where s denotes the active site on the catalyst.

From these different possibilities for steam and methane adsorption listed above, at least six kinetic mechanisms can be postulated. The way in which they are combined and the descriptions of the process are given in Table 5.

Based on information which is well accepted in the literature and the analysis made above, the surface reactions producing CO and CO_2 were assumed as the rate controlling steps (rcs). Among the six possible kinetic mechanisms, the kinetic mechanism 5 was the only one remaining at the end of the model discrimination. Criteria used in the model discrimination will be given later.

9.2. Kinetic mechanism 5

The basic assumptions made for this kinetic mechanism are as follows:

1. H_2O reacts with surface nickel atoms, yielding adsorbed oxygen atoms and gaseous hydrogen.
2. Methane reacts with surface nickel atoms, yielding adsorbed CH_2 radicals and adsorbed H atoms.
3. The adsorbed radicals CH_2 and adsorbed oxygen react to yield adsorbed CHO and adsorbed hydrogen.
4. Adsorbed CHO dissociates to adsorbed CO and H, or reacts with adsorbed oxygen, yielding adsorbed CO_2 and H in parallel.
5. Adsorbed CO reacts with adsorbed oxygen to form CO_2, or desorbs into the gas phase.

Based on these assumptions, the kinetic mechanism 5 can be described by

$$H_2O + s = H_2 + O(s) \quad \text{(m5.1)}$$

$$CH_4 + 3s = CH_2(s) + 2H(s) \quad \text{(m5.2)}$$

$$CH_2(s) + O(s) = CHO(s) + H(s) \quad \text{(m5.3)}$$

$$\text{rcs 1} \quad CHO(s) + s = CO(s) + H(s) \quad \text{(m5.4)}$$

$$\text{rcs 2} \quad CO(s) + O(s) = CO_2(s) + s \quad \text{(m5.5)}$$

$$\text{rcs 3} \quad CHO(s) + O(s) = CO_2(s) + H(s) \quad \text{(m5.6)}$$

$$CO(s) = CO + s \quad \text{(m5.7)}$$

$$CO_2(s) = CO_2 + s \quad \text{(m5.8)}$$

$$2H(s) = H_2 + 2s \quad \text{(m5.9)}$$

Applying the LH–HW approach to the six different kinetic mechanisms, different rate equations can be derived. Accounting for the non-uniform characteristics of the catalyst surface, the concept of Freundlich's non-ideal adsorption is introduced to adjust the powers of steam and hydrogen in the rate equations, which are the main adsorbed components in the system [20]. Because the other five kinetic mechanisms are rejected by the model discrimination done later, only one set of rate equations developed for the kinetic mechanism 5, which remained to the end of the model discrimination, is given for reactions (1)–(3) of Table 1 as follows:

$$r_1 = \frac{k_1(P_{CH_4}P_{H_2O}^{\alpha_{11}}/P_{H_2}^{\alpha_{12}})(1-(P_{CO}P_{H_2}^3/K_{p_1}P_{CH_4}P_{H_2O}))}{(\text{den})^2} \quad (9)$$

$$r_2 = \frac{k_2(P_{CO}P_{H_2O}^{\alpha_{21}}/P_{H_2}^{\alpha_{22}})(1-(P_{CO_2}P_{H_2}/K_{p_2}P_{CO}P_{H_2O}))}{(\text{den})^2} \quad (10)$$

$$r_3 = \frac{k_3(P_{CH_4}P_{H_2O}^{\alpha_{31}}/P_{H_2}^{\alpha_{32}})(1-(P_{CO_2}P_{H_2}^4/K_{p_3}P_{CH_4}P_{H_2O}^2))}{(\text{den})^2} \quad (11)$$

where $\text{den} = 1 + K_{CO}P_{CO} + K_{CO_2}P_{CO_2} + K_H P_H^{0.5} + K_{H_2O}(P_{H_2O}/P_{H_2}) + K_{CH_4}(P_{CH_4}/P_{H_2}) + K_{CHO}(P_{CH_4}P_{H_2O}/$

$P_{H_2}^{2.5}$) and α_{ij} is a adjustable parameter to be determined simultaneously with other parameter estimations for obtaining a suitable model that is statistically and thermodynamically consistent.

Reaction rates for the formation of CO_2 and the disappearance of methane in steam reforming are predicted from

$$r^{o}_{CO_2} = r_2 + r_3, \qquad r^{o}_{CH_4} = r_1 + r_3 \tag{12}$$

Reaction rates for the disappearance of CO_2 and the formation of methane in the reverse water gas shift are predicted from

$$r^{\bullet o}_{CO_2} = r_2 + r_3, \qquad r^{\bullet o}_{CH_4} = r_1 + r_3 \tag{13}$$

9.3. Parameter estimations and model discrimination

Since the experiments were carried out in the integral mode, a non-linear least square analysis was employed for the parameter estimation based on the minimisation of the sum of residual squares of the experimental reaction rates obtained from the Eqs. (5)–(8) and the predicted reaction rates obtained from the Eqs. (12)–(13). A linearisation method was used to solve the problem of non-linear least square analysis [14]. By successive iterations, the estimated values of the parameters can be obtained. The models were discriminated by the physical characterisation of the parameters and comparison among the sums of the residual squares in two steps. First, if one of the main parameters of the model was found to have a negative value, e.g. k_1 or k_3 which should be positive, the model was rejected. The remaining models were then checked by the sum of the residual squares. The t value of a parameter was also employed to consider the parameter's importance in the model [27].

During the experiments of methane steam reforming, reaction (2) was very close to equilibrium as seen from V_2 value in Fig. 10. Also, the partial pressure of CO was low and the adsorption coefficient of H_2 was very small due to a high temperature used. Thus, the rate constant k_2 and adsorption coefficients of K_{CO}, K_H and K_{H_2} could not be estimated significantly from these experiments. In the reverse water gas shift experiments, the partial pressures of CH_4 and H_2O were so low that their adsorption coefficients were only determined from the steam reforming data [27].

The deletion of some adsorption terms in the denominator of the models and the first step of the model discrimination were carried out simultaneously by trial and error. This task was continued until the parameters in the models remaining were found to have correct values corresponding to their physical meanings.

Only the model 5, which has a minimal sum of the residual squares, remained at the end of model discrimination. K_{CO_2}, K_{CH_4} and K_{CHO} did not appear in the model 5 at the end because they were found to have no significant contributions to the model or to have wrong physical characterisations. This may be due to very weak adsorption of CO_2 and CH_4 on the catalyst or to very low concentrations of intermediates CH_2O and CHO.

The final kinetic model based on kinetic mechanism 5 after discrimination is given by

$$r_1 = \frac{k_1(P_{CH_4}P^{0.5}_{H_2O}/P^{1.25}_{H_2})(1-(P_{CO}P^{3}_{H_2}/K_{p_1}P_{CH_4}P_{H_2O}))}{(\text{den})^2} \tag{14}$$

$$r_2 = \frac{k_2(P_{CO}P^{0.5}_{H_2O}/P^{0.5}_{H_2})(1-(P_{CO_2}P_{H_2}/K_{p_2}P_{CO}P_{H_2O}))}{(\text{den})^2} \tag{15}$$

$$r_3 = \frac{k_3(P_{CH_4}P_{H_2O}/P^{1.75}_{H_2})(1-(P_{CO_2}P^{4}_{H_2}/K_{p_3}P_{CH_4}P^{2}_{H_2O}))}{(\text{den})^2} \tag{16}$$

where $\text{den} = 1 + K_{CO}P_{CO} + K_H P^{0.5}_H + K_{H_2O}(P_{H_2O}/P_{H_2})$

The parameters estimated at each temperature in the model are listed in Table 6.

Applying the Arrhenius equation and van't Hoff equation to these parameters for all temperatures

$$k_i = A_i \exp\left(-\frac{E_i}{RT}\right)$$

Table 6
Parameter estimates of the final model

Temperature (K)	$k_1 \times 10^7$ (kmol/kg cat s $(\text{kPa})^{0.25}$)	$k_2 \times 10^5$ (kmol/kg cat s (kPa))	$k_3 \times 10^6$ (kmol/kg cat s $(\text{kPa})^{0.25}$)	$K_{CO} \times 10^2$ $((\text{kPa})^{-1})$	$K_H \times 10^2$ $((\text{kPa})^{-0.5})$	K_{H_2O}
Reverse water gas shift						
598	2.880×10^{-3}	2.708	0.3041	84.91	7.800	
623	1.889×10^{-2}	3.125	0.7675	29.05	4.010	
648	8.081×10^{-2}	3.364	1.713	9.500	1.972	
673	0.3161	3.845	3.469	4.013	1.000	
Methane steam reforming						
748	14.13		24.46			0.7158
773	41.75		45.61			0.7681
798	119.9		74.08			0.8369
823	310.8		123.0			0.9014

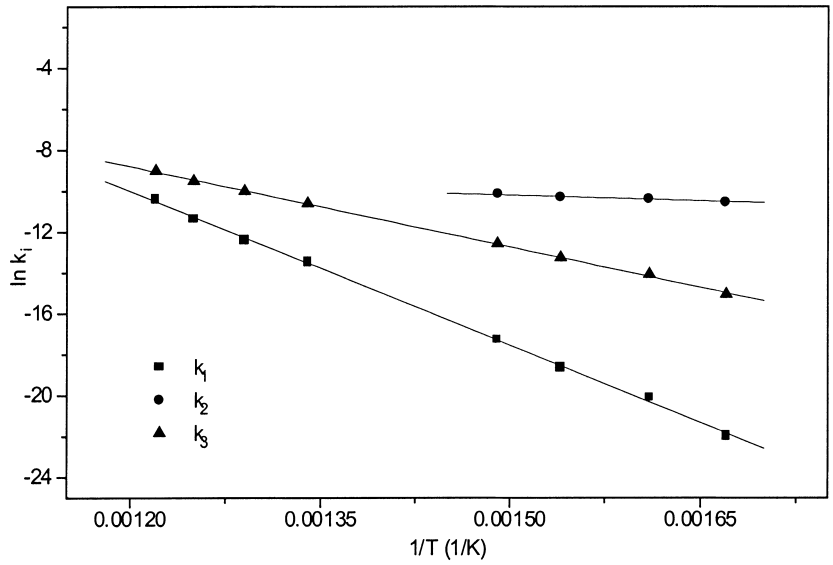

Fig. 13. Temperature dependence of rate constants.

$$K_i = A(K_i)\exp\left(-\frac{\Delta H_{i,a}}{RT}\right)$$

The reaction activation energy E_i and the adsorption enthalpy ΔH_i (heat of chemisorption) of components and the pre-exponential factors A_i and $A(K_i)$ have been determined, and are shown in Figs. 13 and 14, and listed in Table 7.

When the adsorption constant was determined from experimental data, which was based on the chemisorption on an ideal surface or a non-ideal surface or hybrids of the two, it has to satisfy a number of thermodynamic rules [11,18]. Except for steam adsorption, the adsorption constants for carbon monoxide and hydrogen generally satisfy these rules [16].

For H_2O adsorption, from the results reported elsewhere and reviewed by Rostrup-Nielsen [23], it was concluded that the catalyst support plays a very important role in its adsorption. Thus, the step written

$$H_2O + s = O(s) + H_2 \quad \text{(s1)}$$

consists of the following steps:

$$H_2O + s = H_2O(s) \quad \text{(s2)}$$

$$H_2O(s) + s = O(s) + H_2 + s \quad \text{(s3)}$$

The support enhances adsorption of steam which is then adsorbed on the nickel surface. Since steam is also adsorbed

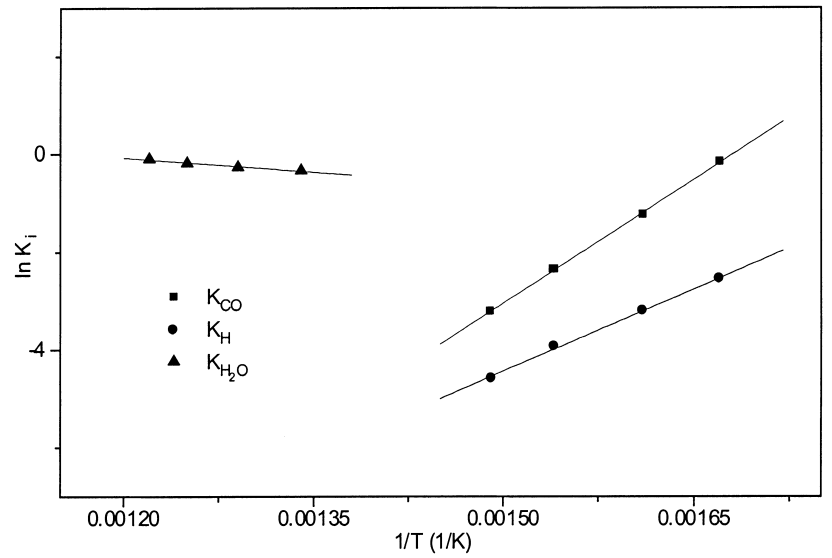

Fig. 14. Temperature dependence of adsorption parameters.

Table 7
Activation energies, adsorption enthalpies and pre-exponential factors for the final model

	E_1 (kJ/mol)	E_2 (kJ/mol)	E_3 (kJ/mol)	$\Delta H_{CO,a}$ (kJ/mol)	$\Delta H_{H,a}$ (kJ/mol)	$\Delta H_{H_2O,a}$ (kJ/mol)
t-value	209.2 (82.4)	15.4 (8.32)	109.4 (55.0)	−140.0 (63.6)	−93.4 (25.2)	15.9 (11.4)
UL[a]	214.2	19.0	111.8	−135.7	−86.1	18.6
LL[b]	204.2	11.8	107.0	−144.3	−100.7	13.2
	A_1	A_2	A_3	$A(K_{CO})$	$A(K_H)$	$A(K_{H_2O})$
	5.922×10^{8}	6.028×10^{-4}	1.093×10^{3}	5.127×10^{-13}	5.68×10^{-10}	9.251

[a] UL = upper limit.
[b] LL = lower limit of approximate 95% confidence interval.

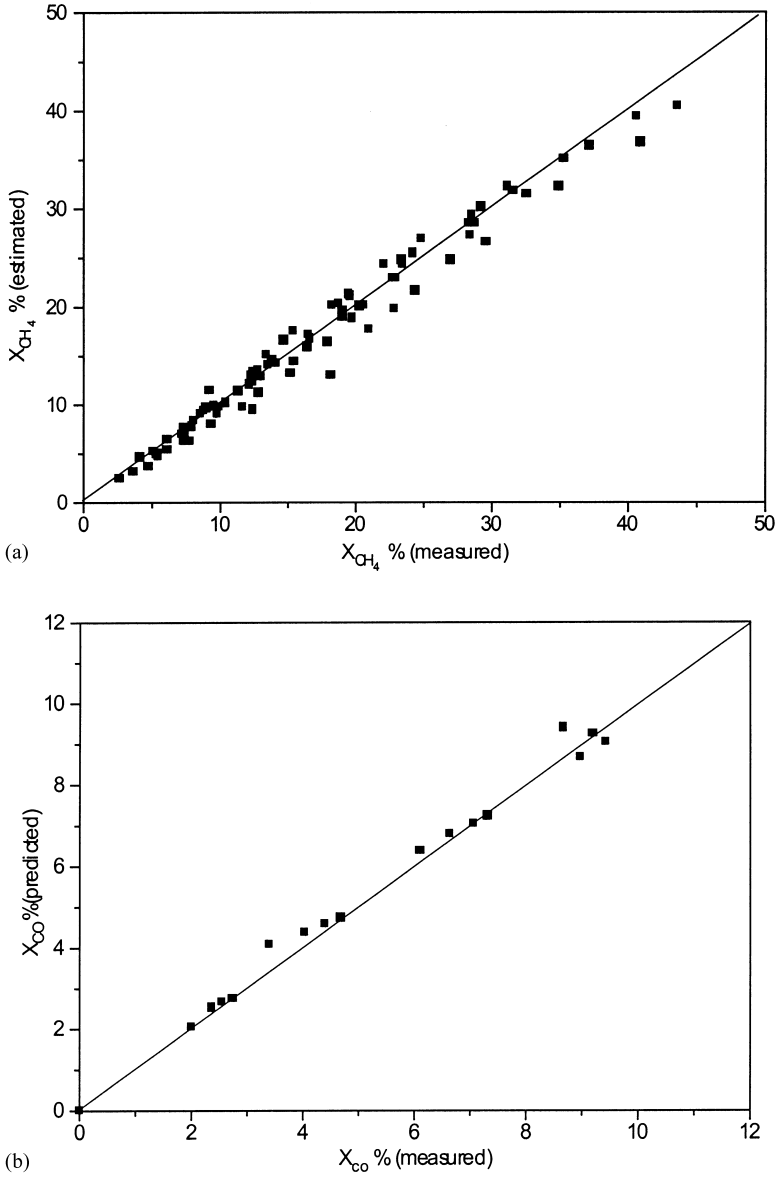

Fig. 15. (a) Comparison between X_{CH_4} (measured) and X_{CH_4} (estimated); methane steam reforming. (b) Comparison between X_{CO_2} (measured) and X_{CO_2} (estimated), reverse water gas shift reaction.

directly on the nickel surface as in step (s1), the K_{H_2O}, which appears in the model that has been taken into consideration steam adsorption, cannot be considered a true equilibrium constant. In fact, it only reflects a steady-state condition reached by the steps involved in s1–s3. Thus, K_{H_2O} can be written as

$$K_{H_2O} = K_{s2}\frac{k_{s3}}{k_{-s1}}$$

where K_{s2} is the equilibrium constant of step s2, K_{s3} the direct kinetic constant of step s3, k_{-s1} the reverse kinetic constant of step s1. As stated above, K_{H_2O} cannot be considered a real equilibrium constant and in consequence does not follow the rule discussed above.

10. Model verification

The model verification was carried out in an integral mode. In order to derive the model that describes the experimental reactor, the following assumptions have been made:

1. Steady state operation.
2. Isothermal conditions prevail.
3. Negligible pressure drop.
4. Plug flow in the reactor.
5. No interphase and intraparticle mass transfer limitations.

Assumption 5 was confirmed by the experiments of size variation of the catalyst particle and the theoretical calculation done [16]. Assumption 2 also holds due to the very small amount and very small size of the catalyst used. Also a maximum pressure drop of 20 Pa was obtained throughout the whole reactor at the maximum flow rate during the experiments. Since the length of catalyst loaded (0.25–0.4 cm) is very small, compared with the reactor length (20.5 cm), the neglect of pressure drop through the catalyst bed is reasonable. Assumption 4 could be accepted under the conditions of high temperatures and low pressures used.

Based on these assumptions, a mathematical model can be written for all components as follows:

$$\frac{dn_i}{dl} = \Omega\rho_B\sum_{j=1}^{3}\nu_{ij}r_j \tag{17}$$

where $i = 1, 2, 3, 4$ and 5 for CH_4, H_2O, CO, CO_2 and H_2, respectively, ν_{ij} the stoichiometric coefficient of component i in reaction j, Ω the cross-sectional area of the catalyst bed.

The initial conditions for the model are

$$L = 0, \qquad n_i = n_i^i \tag{18}$$

and the model was solved by the fourth Runge–Kutta method.

The comparisons between the values predicted and the measured experimentally for methane steam reforming and reverse water gas shift at different conditions are presented in Fig. 15a and b, respectively. It is clear that the values predicted and the values measured experimentally are in good agreement.

11. Conclusions

An experimental study on methane steam reforming has been carried out on a commercial catalyst (ICI 57-4) over wide ranges of operational parameters, but still within a region of intrinsic kinetics. Under low methane conversion and low temperature, the rate of reaction of methane with steam is first-order with regard to methane, which is suggested by methane conversion being proportional to the contact time and the partial pressure of methane. Temperature and the ratio of steam to methane had a large effect on the product distribution and no noticeable effect of pressure on it was observed. The experimental results indicate that a high ratio of steam to methane and low temperature are favourable to the production of hydrogen and synthesis gas. The rate of carbon dioxide formation is much faster than that of carbon monoxide at low temperature. This may imply that the reaction $CH_4 + 2H_2O = CO_2 + 4H_2$ is dominant to methane steam reforming on the catalyst used at low temperature. However, both carbon dioxide and carbon monoxide are primary reaction products, which is concluded from a trend of carbon dioxide selectivity not approaching one at low methane conversion. In other words, the reaction $CH_4 + H_2O = CO + 3H_2$ does take place simultaneously. Based on the trend of carbon dioxide selectivity, it can be expected that the domination of the former reaction will decrease with temperature.

A kinetic model for the commercial Ni/α-Al_2O_3 catalyst (ICI 57-4) has been developed, based on the mechanism that both methane and steam are adsorbed on the catalyst with dissociation, with the methane dissociated into CH_2 and H_2 or adsorbed H, and the suggestion that surface reactions between adsorbed species are rate controlling. The mechanism and kinetic model developed differs from those of [25,27] due to the different catalyst used. This kinetic model gives a reasonable representation of the experimental data obtained on the catalyst used, and also predicts a detailed product distribution of steam reforming. Combining the model with a consideration of mass and heat transfer limitations encountered when large catalyst particles are used, the intrinsic kinetic model presented here may be employed in the simulation and comprehensive analysis of an industrial reformer loaded with the same catalyst.

Acknowledgements

We gratefully acknowledge ICI Kalatco for supply of the catalyst, catalyst micromeritic data and financial support for this work.

References

[1] M.E. Agnelli, M.C. Demicheli, E.N. Ponzi, Catalytic deactivation on methane steam reforming catalysts: 2. Kinetics study, Ind. Eng. Chem. Res. 26 (1987) 1707–1713.

[2] W.W. Akers, D.P. Camp, Kinetics of methane–steam reforming, AIChE J. 1 (1955) 471–475.

[3] A.S. Al-Ubaid, Methane steam reforming activity, stability and characterisation of nickel catalysts, Ph.D. Thesis, University of Notre Dame, IN, USA, 1984.

[4] A.S. Al-Ubaid, S.S.E.H. Elnashaie, M. Abashar, Methane Conversion, Elsevier, New York, 1988.

[5] D.W. Allen, E.R. Gerhard, M.R. Likins Jr., Kinetics of the methane–steam reaction, Ind. Eng. Chem. Proc. Des. Dev. 14 (3) (1975) 256–259.

[6] L. Aparicio, Transient isotopic studies and microkinetic modelling of methane reforming over nickel catalysts, J. Catal. 165 (1997) 262–274.

[7] R.W. Blue, V.C.F. Holm, R.B. Regier, F. Edwin, L.F. Heckelsberg, Effect of granule size: in dehydrogenation and in hydrogen transfer reactions, Ind. Eng. Chem. 44 (1952) 2710–2715.

[8] N.M. Bodrov, L.O. Apelbaum, M.I. Temkin, Kinetics of the reactions of methane with steam on the surface of nickel, Kinet. Catal. 5 (1964) 696–705.

[9] N.M. Bodrov, L.O. Apelbaum, M.I. Temkin, Kinetics of the reaction of methane with water vapour, catalysed nickel on a porous carrier, Kinet. Catal. 8 (1967) 821–828.

[10] N.M. Bodrov, L.O. Apelbaum, M.I. Temkin, Kinetics of the reactions of methane with steam on the surface of nickel at 400–600°C, Kinet. Catal. 9 (1968) 1065–1071.

[11] J.B. Butt, Reaction Kinetics and Reactor Design, Prentice-Hall, Englewood Cliffs, NJ, 1980, 169 pp.

[12] J.C. De Deken, E.F. Devos, G.F. Froment, Steam Reforming of Natural Gas, Chem. React. Eng. ACS Symp. Ser., 1982, 196 pp.

[13] H.A. Dirksen, C.H. Riesz, Equilibrium in the steam reforming of natural gas, Ind. Eng. Chem. 45 (7) (1953) 1562–1565.

[14] N.R. Draper, H. Smith, Applied Regression Analysis, 2nd Edition, Wiley, New York, 1981, 462 pp.

[15] G.F. Froment, K.B. Bischoof, Chemical Reactor Analysis and Design, Wiley, New York, 1979, 110 pp.

[16] K. Hou, Experimental study of intrinsic kinetics and diffusion during methane steam reforming, Ph.D. thesis, The University of Salford, UK, 1998.

[17] R. Kopsel, A. Richter, B. Meyer, Catalyst deactivation and kinetics of methane steam reforming, Chem. Tech. 32 (1980) 460.

[18] H.H. Lee, Heterogeneous Reactor Design, Butterworth Publishers, Stoneham, MA, 1985, 66 pp.

[19] A.E.C. Luna, A.M. Becerra, Kinetics of methane steam reforming on a Ni on alumina–titania catalyst, React. Kinet. Catal. Lett. 61 (2) (1997) 369–374.

[20] Toru Numaguchi, Kikuchi Katsutoshi, Intrinsic kinetics and design simulation in a complex reaction network: steam–methane reforming, Chem. Eng. Sci. 43 (1988) 2295–2301.

[21] P.T. Quach, U.D. Rouleau, Kinetics of the methane–steam reaction over nickel catalyst in a continuous stirred tank reactor, J. Appl. Chem. Biotechnol. 25 (1975) 445–459.

[22] J.R.H. Ross, M.C.F. Steel, Mechanism of the steam reforming of methane over a copreciptated nickel-alumina catalyst, J. Chem. Soc., Faraday Trans. 1 (1972) 69.

[23] J.R. Rostrup-Nielsen, Catalytic Steam Reforming, Springer, Berlin, 1984.

[24] C.N. Satterfield, Heterogeneous Catalysis in Practice, McGraw-Hill, New York, 1980, 349 pp.

[25] M.A. Soliman, M.A. Adris, A.S. Al-Ubaid, S.S.E.H. El-Nashaie, Intrinsic kinetics of nickel/calcium aluminate catalyst for methane steam reforming, J. Chem. Tech. Biotechnol. 55 (1992) 131–138.

[26] M.V. Twigg, Catalyst Handbook, 2nd Edition, Wolfe Publishing Ltd., UK, 1989.

[27] J. Xu, G.F. Froment, Methane–steam reforming, methanation and water gas shift — I. Intrinsic kinetics, AIChE J. 35 (1989) 88–96.